A Compact Source for Quasi-periodic Pulsation in an M-class Solar Flare

Ding Yuan[1,2] , Song Feng[3,4] , Dong Li[5] , ZongJun Ning[5], and Baolin Tan[2]

[1] Institute of Space Science and Applied Technology, Harbin Institute of Technology, Shenzhen, Guangdong 518055, People's Republic of China
yuanding@hit.edu.cn
[2] Key Laboratory of Solar Activity, National Astronomical Observatories, Chinese Academy of Sciences, Beijing 100012, People's Republic of China
[3] Yunnan Astronomical Observatory, Chinese Academy of Sciences, P.O. Box 110, Kunming 650011, People's Republic of China
[4] Yunnan Key Laboratory of Computer Technology Application, Faculty of Information Engineering and Automation, Kunming University of Science and Technology, Kunming 650500, People's Republic of China
[5] Key Laboratory for Dark Matter and Space Science, Purple Mountain Observatory, Chinese Academy of Sciences, Nanjing 210034, People's Republic of China
Received 2019 September 12; revised 2019 November 12; accepted 2019 November 12; published 2019 November 22

Abstract

Quasi-periodic pulsations (QPPs) are usually found in the light curves of solar and stellar flares; they carry the features of time characteristics and plasma emission of the flaring core, and could be used to diagnose the coronas of the Sun and remote stars. In this study, we combined the Atmospheric Imaging Assembly (AIA) on board the *Solar Dynamics Observatory* and the Nobeyama Radioheliograph (NoRH) to observe an M7.7 class flare that occurred at active region 11520 on 2012 July 19. A QPP was detected both in the AIA 131 Å bandpass and the NoRH 17 GHz channel; it had a period of about four minutes. In the spatial distribution of Fourier power, we found that this QPP originated from a compact source and that it overlapped with the X-ray source above the loop top. The plasma emission intensities in the AIA 131 Å bandpass were highly correlated within this region. The source region is further segmented into stripes that oscillated with distinctive phases. Evidence in this event suggests that this QPP was likely to be generated by intermittent energy injection into the reconnection region.

Unified Astronomy Thesaurus concepts: Magnetohydrodynamics (1964); Solar flares (1496); Active solar corona (1988)

1. Introduction

Quasi-periodic pulsation (QPP) is a rhythmic modulation to electromagnetic radiation of plasma in a wide range of frequencies during a solar or stellar flare. It is normally observed in integrated light curves in most electromagnetic bandpasses of solar and stellar plasma emissions, ranging from radio band, visible light, extreme ultraviolet (EUV) to X-rays (see reviews of Nakariakov & Melnikov 2009; Van Doorsselaere et al. 2016). Statistics with *Geostationary Operational Environmental Satellite* (*GOES*) soft X-ray emission suggests that 80% of the solar flares exhibit QPP during the impulsive phase (Simões et al. 2015). Since QPP carries the time characteristics of flare emission, it could be used to diagnose the key parameters of the flaring site (e.g., Brosius & Daw 2015; Pugh et al. 2019).

Two theories are proposed to explain the origin of QPP in a flare: repetitive magnetic reconnection (McLaughlin et al. 2009, 2012; Thurgood et al. 2017; Dominique et al. 2018; McLaughlin et al. 2018) and modulation to the flaring site by magnetohydrodynamic (MHD) waves (Nakariakov et al. 2006; Reznikova & Shibasaki 2011; Tian et al. 2016). Repetitive magnetic reconnection cannot be observed directly, since the coronal magnetic field is extremely difficult to measure with current instrumentation. Moreover, the dynamics of a current sheet, which is a direct byproduct of magnetic reconnection, does not normally reveal itself in the EUV emissions of coronal plasma. Albeit difficult, several studies attempted to estimate the magnetic field or current sheet with lucky viewing angles in imaging or spectroscopic measurement (Su et al. 2013; Longcope et al. 2018; Warren et al. 2018). To investigate the physics of QPP, one has to seek the signature of repetitive waves and flows during magnetic reconnection (McLaughlin et al. 2012).

If one suggests the modulation by MHD waves, a plausible step is to correlate the time stamps in integrated light curves and periodic waves. A series of studies was done on modulation by standing and reflective slow mode waves (Wang et al. 2003a, 2003b; Wang 2011; Kumar et al. 2013, 2015; Fang et al. 2015; Yuan et al. 2015; Mandal et al. 2016). Most previous studies focus on a good match of periodicity and phase difference. However, after the nine-year launch of the *Solar Dynamics Observatories* (*SDO*; Pesnell et al. 2012), although its onboard instrument—the Atmospheric Imaging Assembly (AIA; Lemen et al. 2012) has sufficient spatial and temporal resolutions in nine UV and EUV channels, no observation provides convincing evidence on the causality between an MHD wave and QPP. Therefore, the attempts to diagnose the reconnection site of solar and stellar flares with QPP are weakly supported (e.g., Kim et al. 2012).

A correct model is extremely nontrivial for stellar flare QPP, since the spatial resolution is not achievable for a remote star. Once the nature of QPP is justified, it would become a novel tool to diagnose stellar atmospheres. In this study, we found that QPP originates from a very compact source above the loop top, and that no connectivity was found between QPP and other oscillatory signals at the lower atmosphere. This Letter is structured as follows: Section 2 presents data preparation and methods; Section 3 describes the main results and is followed by a discussion in Section 4.

2. Data Reduction and Analysis

On 2012 July 19, a *GOES* class M7.7 flare was detected in NOAA active region (AR) 11520. This AR has rotated to the west limb of the Sun, an arcade of coronal loops was well oriented for observation in both EUV and radio emission bandpasses (Figures 1(b) and (c)). Figure 1(a) presents the
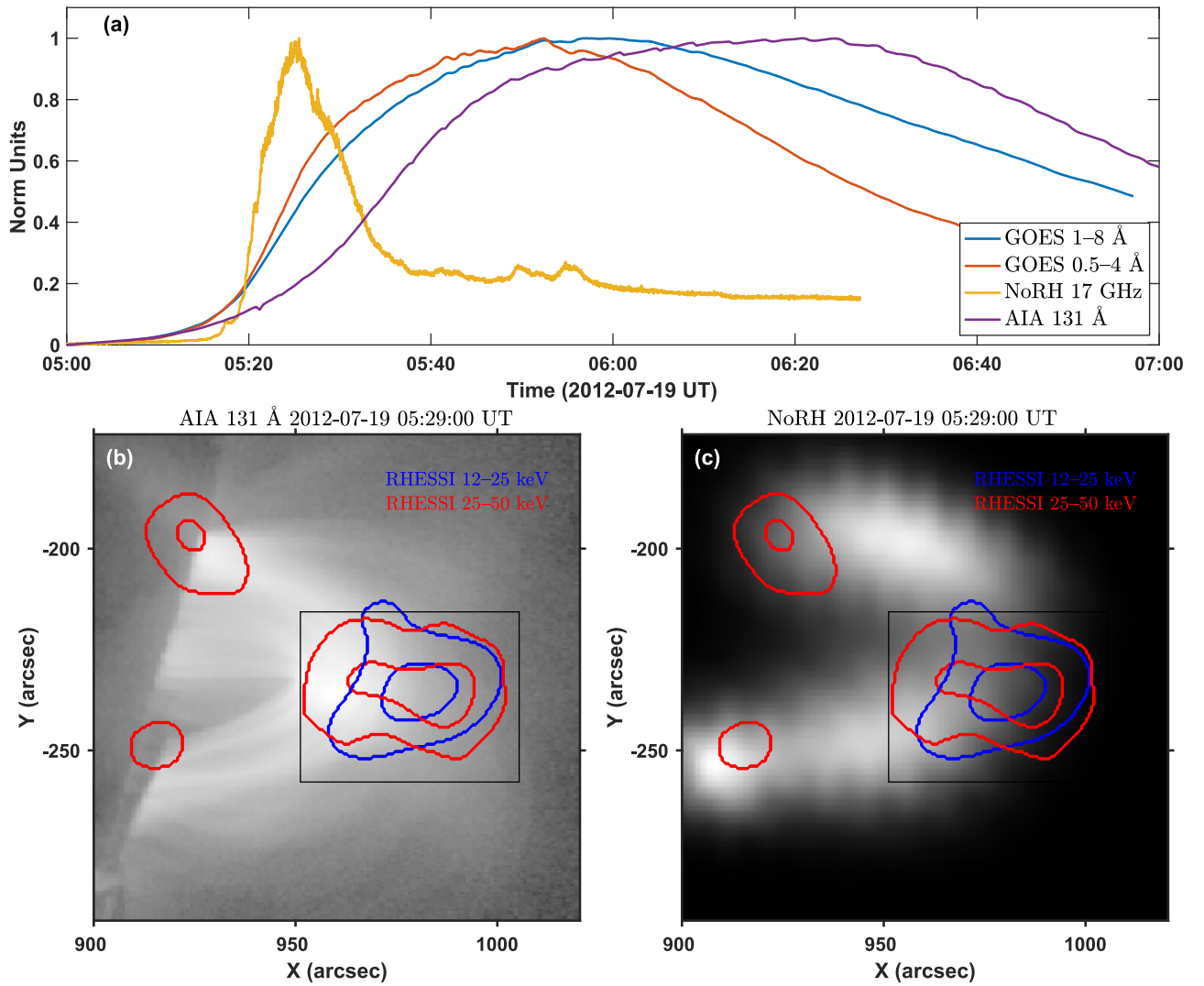
Figure 1. An arcade of loops at AR 11520 recorded by the AIA 131 Å channel (b) and NoRH 17 GHz band (c) at 06:10 UT on 2012 July 19. The *RHESSI* X-ray emission intensity was overlaid with contour levels at 50% and 90% of the peak intensity. Two energy bands were computed at 12–25 keV (blue) and 25–50 keV (red), respectively. (a) Light curves of the *GOES* SXR flux at 1–8 Å, 0.5–4 Å; the NoRH radio flux at 17 GHz; and the AIA 131 Å bandpasses. They are normalized to the peak value so that the maximum value is one. The AIA 131 Å signal was averaged over the rectangle at the loop top as marked in panel (b).

Soft X-ray fluxes recorded by *GOES*, the average EUV emission intensity captured by the AIA 131 Å channel, and the average radio flux at 17 GHz received by the Nobeyama Radioheliograph (NoRH; Nakajima et al. 1994). The soft X-ray flux started to raise at about 4:17 UT, reached a peak value at about 6:00 UT, and decayed off gradually. The NoRH 17 GHz radio flux rapidly raised to peak value and decayed off from about 5:15 UT to about 5:40 UT. Figure 1(a) reveals QPPs in the soft X-ray fluxes and the average EUV emission close to the peak time of this flare. No apparent QPP was visible in the NoRH 17 GHz signal; however, we will show later that significant periodic signal was buried in this light curve.

The magnetic structure of this AR was well exposed for investigating solar flare models and its dynamics at the outer corona; several articles were published to report various aspect of this flare and the associated dynamics. Liu et al. (2013) measured the plasmoid ejections and sought evidence of particle acceleration during magnetic reconnection; Sun et al. (2014) studied the thermal structure of flaring loops; Liu (2013) investigated the currents behind an erupting flux rope; Patsourakos et al. (2013) reported evidence of a fast

coronal mass ejection driven by the prior information of a magnetic flux rope. Wu et al. (2016) used Nobeyama Radioheliograph data to study the nonthermal electron emissions; they detected an intermittent timescale of about 2 minutes for magnetic reconnection. More specifically, Huang et al. (2016) reported quasi-periodic acceleration of electrons that may coincide in the bidirectional outflows from the reconnection region.

SDO/AIA data have excellent spatial and temporal resolutions that reveal the source and time characteristics of this QPP. The AIA data were calibrated with the standard calibration routine provided by the SolarSoft package.[6] The digital offset for the cameras, CCD readout noise, and dark current were removed from the data, then each image was corrected with a flat-field and was normalized with its exposure time. The saturated images were disregarded, so the cadence is reduced to 24 s in the EUV data. NoRH recorded the 17 GHz radio flux until 6:27 UT; the cadence was fixed to 1 s.
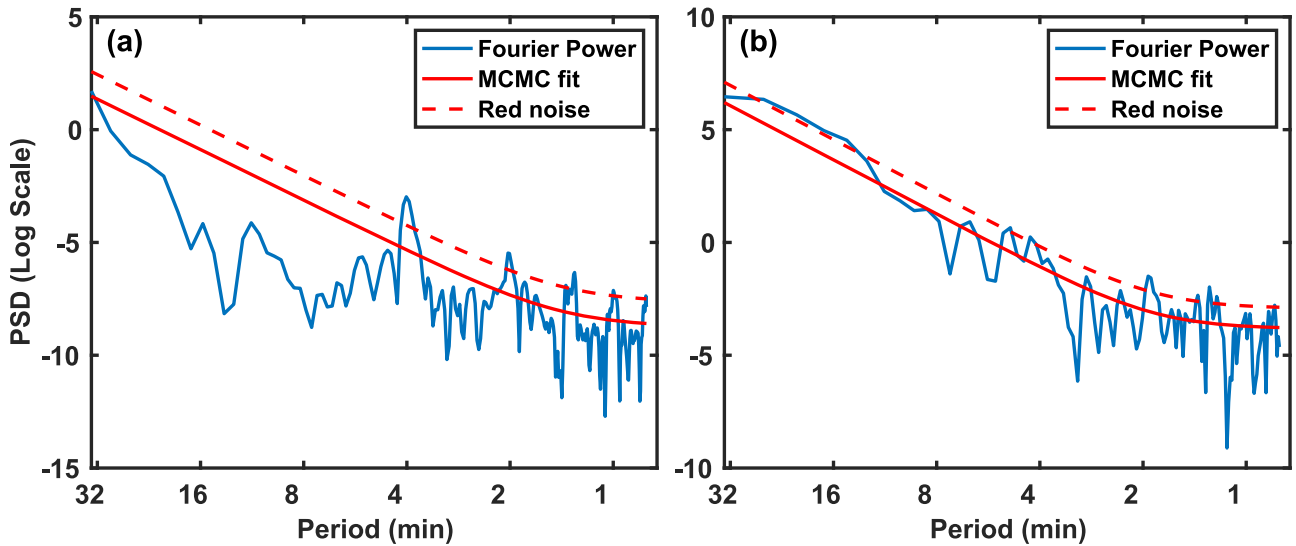
---

[6] http://www.mssl.ucl.ac.uk/surf/sswdoc/solarsoft/

Figure 2. Fourier power spectra of the light curves of the AIA 131 Å bandpasses (a) and the NoRH radio flux at 17 GHz (b) as shown in Figure 1(a). The Markov Chain Monte Carlo (MCMC) fit and red noise at the 95% confidence level (or 5% significance level) are overplotted as a guideline for assessing significant oscillatory signals.
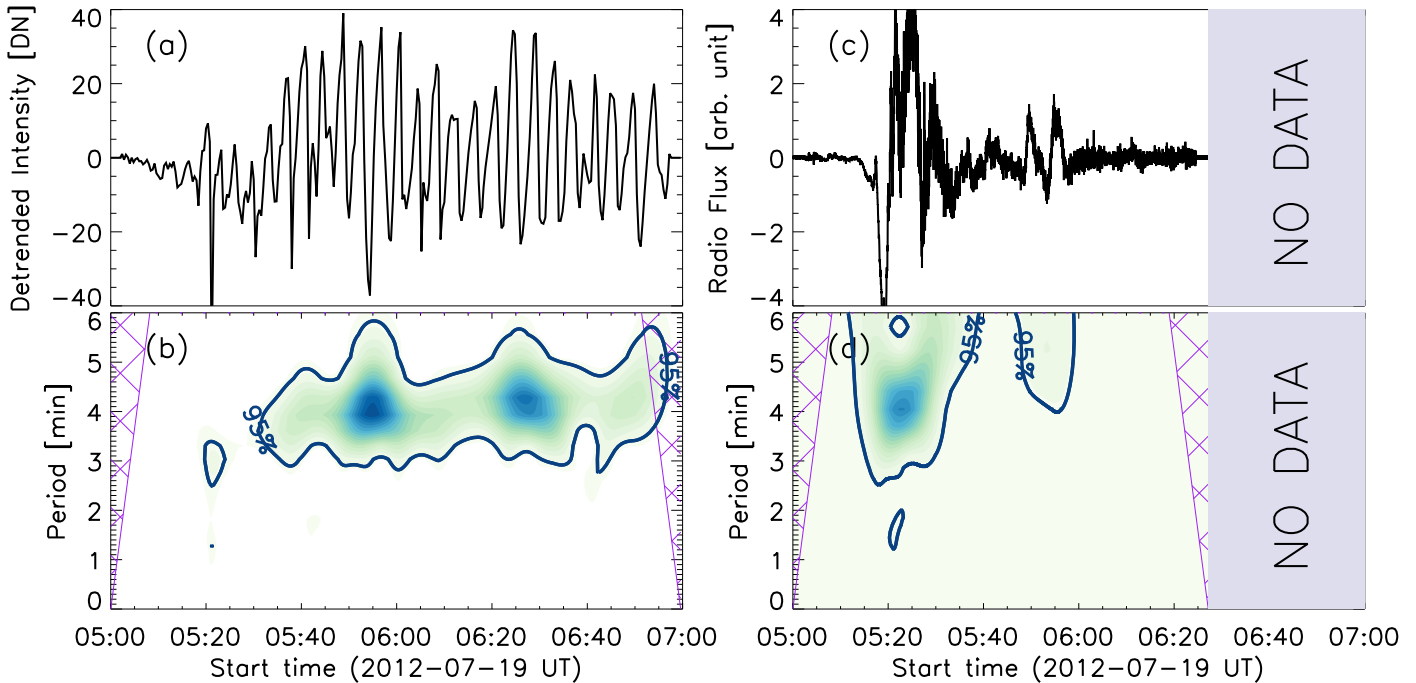

Figure 3. (a) Light curve of the average 131 Å signal after removing the 5 minute moving average. (b) Wavelet power spectrum. Panels (c) and (d) are the same analysis as the NoRH 17 GHz radio flux. The contours in (b) and (d) are the 95% confidence level (or 5% significance level). The cones of influence are cross-hatched; they represent the meaningless power affected by zero-paddings.

We used *RHESSI* (Lin et al. 2002) detectors 3 and 5–9, and the CLEAN algorithm to compute the X-ray images. The measurement started on 5:29:30 UT and integrated for 30 s. The contours of X-ray emission intensity were overlaid in Figures 1(b), (c), and 4(a).

Figure 1(a) plots the EUV emission intensity variation in the AIA 131 Å channel; this signal was averaged within the area enclosed by the black rectangle (Figure 1(b)). We estimated the global trend by taking the 5 minute moving average, and removed it from the light curve to highlight the periodic pulsations.

Some researchers are concerned about the effect of detrending, so they developed a robust spectral method to detect oscillatory signals in the original light curves (e.g., Gruber et al. 2011; Inglis et al. 2015; Pugh et al. 2017). These algorithms could reveal significant oscillatory signals within a Fourier spectrum, which normally follows a power-law distribution. This practice could appropriately account for the red noise in the data (Pugh et al. 2017). We calculated the Fourier spectra with the original light curves of both the 131 Å and 17 GHz fluxes, and assessed the significance level with the red noise distribution and Markov Chain Monte Carlo
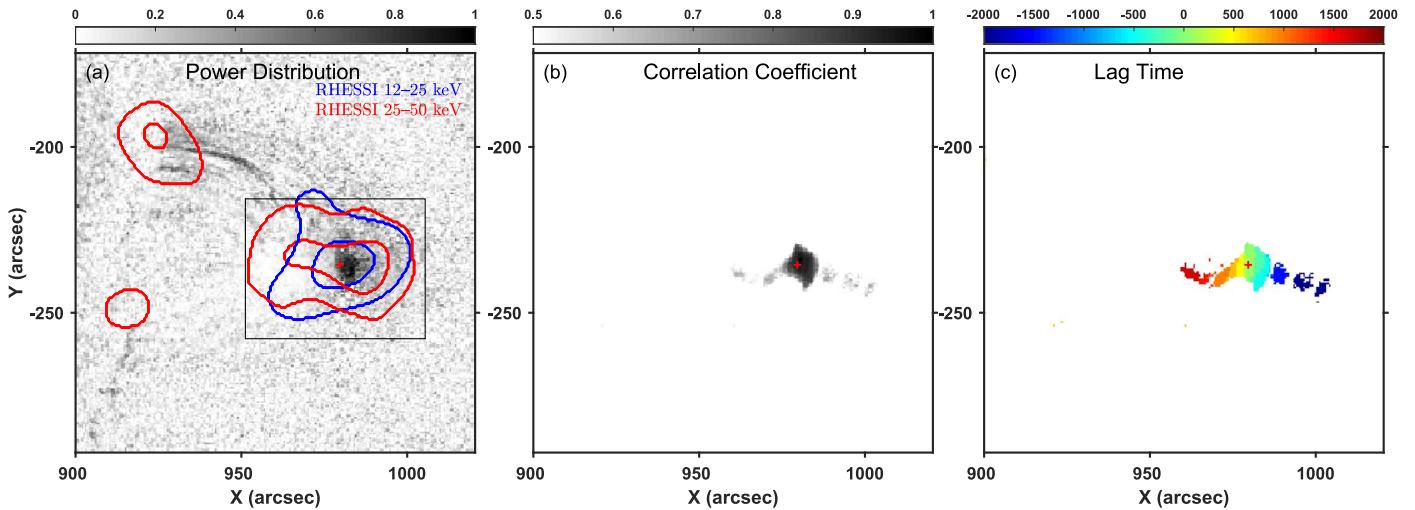
Figure 4. (a)–(c) Maps of Fourier power averaged between 200 and 300 s, correlation coefficient, and lag time. The red plus symbol represents the reference pixel. Panel (a) only draws the pixel with a 4 minute oscillation above the 3σ white-noise level. The contours in (a) are the same as plotted in Figure 1.

(MCMC) fit (see Figure 2). These results confirmed that the 4 minute oscillation analyzed throughout this study is above the 95% confidence level in both the AIA 131 Å and NoRH 17 GHz signals. We also note a significant spectral peak with a 2 minute periodicity, but its amplitude is very small, so it is hardly detectable in the wavelet spectrum (see Figure 3). We hereafter opt to use a wavelet analysis with a detrended times series, so that the temporal behavior and the connectivity between different observables could be examined.

The detrended time series was plotted in Figure 3(a) and was analyzed with a wavelet transform (Torrence & Compo 1998); the wavelet spectrum was plotted in Figure 3(b). Similar analysis was done to the NoRH 17 GHz data; the time series and wavelet spectrum were plotted in Figures 3(c) and (d), respectively.

To study the spatial distribution of QPP, we perform Fourier transform to the detrended emission intensity of every pixel in the AIA 131 Å and average the Fourier power among the spectral components between 200 and 300 s (Figure 4(a)). This range includes significant periodic signals revealed in Figure 3(b). Before this step, we removed the 5 minute moving average in each time series as done in the wavelet analysis. Within each pixel, we estimate the white-noise level for the Fourier power spectrum according to Torrence & Compo (1998). Figure 4(a) only presents the pixels with a 4 minute oscillation power above the 3σ noise level. In the NoRH 17 GHz images, the loop-top emission was very weak (Figure 1). The plasma density and temperature were significantly enhanced above the loop top (Huang et al. 2016; Wu et al. 2016); therefore, the opacity for the 17 GHz emission varies between footpoints and loop top. So similar analysis to the NoRH data set could not effectively reveal the spatiotemporal knowledge about the source above the loop top. Our event is different from the case studied in Inglis et al. (2008), in which the coronal loops had a very different orientation (see Figure 6 in Inglis et al. 2008).

We note that the region with QPP was very compact and only localized above the loop top. To reveal the intercorrelation within the source region, we calculated the cross-correlation coefficient (XC) of the detrended emission intensity of each pixel and that of a reference pixel at the loop top as labeled in Figure 4. We measured the lag time by finding the argument maximum of XC for each pixel; the maximal XC and lag time within the region of interest are illustrated in Figures 4(b) and (c).

3. Results

During this M7.7 flare, we observed several QPPs with distinct periods in the soft X-ray, radio, and EUV emission light curves; Huang et al. (2016) report a thorough study on the quasi-periodic processes. In this study, we focus on the spatiotemporal characteristics of QPP in the EUV imaging data. This sort of study was attempted with NoRH radio observation (e.g., Fleishman et al. 2008; Inglis et al. 2008); however, the coarse spatial resolution of radio observation is not sufficient to reveal the fine structure of QPP. With a thorough understanding of QPP in solar flares, we could apply the knowledge to stellar flares with QPP and derive more details of a remote star.

Figure 1(a) shows that in the averaged 131 Å light curve quasi-periodic signals were clearly visible from about 5:30 to 7:00 UT. Figures 3(a) and (b) represent, respectively, the detrended signal and its wavelet power spectrum. A significant period is detected at about 4 minutes; the periodicity lasts persistently for about 90 minutes. We also detected an oscillatory signal with the same periodicity in the NoRH 17 GHz radio signal (Figures 3(c) and (d)); however, this QPP only lasted from 5:15 UT to 5:40 UT. It occurred about 15 minutes ahead of the EUV signal; two oscillatory signals had an overlap of about 10 minute duration (or 2.5 oscillatory cycles).

Figure 4(a) presents the Fourier power distribution of the 4 minute periodicity. We found that this 4 minute oscillation was only significant above the loop top, and its spatial extent was compact and had an overlap with the hard X-ray emission region. Moreover, these oscillations were highly correlated, and the XC coefficient was greater than 0.5 in the compact region above the loop top; see Figure 4(b). Figure 4(c) reveals that this oscillation could be segmented into several subregions. Within each subregion the lag time was uniform. However, between two neighboring subregions, the lag time had a difference of about 200–300 s, which is very close to an oscillation cycle.

4. Discussions

In this study, an arcade of loops at AR 11520 was well oriented for observation. An M7.7 flare was detected on 2012 July 19 at this AR. During this flare, QPP was detected both in the light curves of the AIA 131 Å bandpass and the NoRH 17 GHz radio flux. The emission intensities oscillated with a period of about 4 minutes.

The QPP had a very compact source and was only localized above the loop top. Its location had an overlap with the hard X-ray source above the loop top. The QPP source region exhibited high correlation and was segmented into several stripes according to the distribution of lag time.

The oscillatory signal in the NoRH 17 GHz started about 15 minute ahead of the AIA 131 Å signal. The order of start time of the two detected oscillatory signals implies that this QPP might be triggered by an energetic process, which was first observed in high energy radiation and then detectable in the EUV emissions. The QPP in the AIA 131 Å channel did not exhibit significant damping during a 90 minute interval. Similar persistent QPPs were detected at the impulsive phase and decay phase of an X8.2 solar flare (Hayes et al. 2019). This feature is contradictory to those QPPs with strong damping (e.g., Anfinogentov et al. 2013). So this kind of QPP should be driven periodically or by a sequence of impulsive energy injections.

If we consider the periodicity at the MHD timescale and its persistence, such a signal resembles the leakage of sunspot oscillations (Yuan et al. 2011, 2016; Li et al. 2018). However, we did not observe a similar oscillatory signal propagating along the loops in the EUV emission intensity (see Figure 4(a)), so we rule out the possibility of leakage of sunspot oscillation in the form of a slow mode wave. If such leakage is the cause, the propagation of energy should not disturb the density or temperature of the flaring loop, and then it could be nonthermal particles or Alfvén waves. Chen & Priest (2006) demonstrated that the solar p-mode could modulate the reconnection site and generate an oscillatory signal. However, we did not find sufficient evidence to support this theory in this event.

This QPP is also likely to be caused by self-consistent periodic modulation to the energy releasing site at the loop top by colliding flows or nonthermal plasma. Such a scenario is reproduced by MHD simulations (Fang et al. 2016; Ruan et al. 2019). Ruan et al. (2019) simulated a turbulent flare loop by triggering counter-streaming flows at the loop top and reproduced a compact QPP source with high correlations.

Another possible origin is the intermittent bombardment of quasi-periodic plasmoid generated by magnetic reconnections. This process was numerically predicted by Takasao & Shibata (2016) and Zhao et al. (2019). The event studies in this Letter are more inclined to support this origin. Wu et al. (2016) detected a 2 minute periodicity in the pre-impulsive phase of the same flare; this periodicity is about half of the period measured in this study. In our study, we also detect significant 2 minute oscillation, but its amplitude was very small compared to the 4 minute oscillation (see Figures 2 and 3). The 2 minute oscillations in the impulsive and decay phases might be connected to the signal in the pre-impulsive phase as presented in Wu et al. (2016), but we do not have conclusive evidence at this stage. Such a rhythmic process is accompanied by a fast contracting loop and upward ejective plasmoids (Liu et al. 2013). This scenario appears to be consistent with the lag time distribution (Figure 4(c)).

In this study, we report both the spatial extent and causality of a QPP. Although the physical mechanism of QPP is not conclusive, we obtained a wealth of new features about QPP. It is a good start for future investigations. A combination of imaging and spectroscopic study should be able to get insight into the origin of this kind of QPP.

ORCID iDs

Ding Yuan ⓘ https://orcid.org/0000-0002-9514-6402
Song Feng ⓘ https://orcid.org/0000-0003-4709-7818
Dong Li ⓘ https://orcid.org/0000-0002-4538-9350
Baolin Tan ⓘ https://orcid.org/0000-0003-2047-9664

References

Anfinogentov, S., Nakariakov, V. M., Mathioudakis, M., Van Doorsselaere, T., & Kowalski, A. F. 2013, ApJ, 773, 156
Brosius, J. W., & Daw, A. N. 2015, ApJ, 810, 45
Chen, P. F., & Priest, E. R. 2006, SoPh, 238, 313
Dominique, M., Zhukov, A. N., Dolla, L., Inglis, A., & Lapenta, G. 2018, SoPh, 293, 61
Fang, X., Yuan, D., Van Doorsselaere, T., Keppens, R., & Xia, C. 2015, ApJ, 813, 33
Fang, X., Yuan, D., Xia, C., Van Doorsselaere, T., & Keppens, R. 2016, ApJ, 833, 36
Fleishman, G. D., Bastian, T. S., & Gary, D. E. 2008, ApJ, 684, 1433
Gruber, D., Lachowicz, P., Bissaldi, E., et al. 2011, A&A, 533, A61
Hayes, L. A., Gallagher, P. T., Dennis, B. R., et al. 2019, ApJ, 875, 33
Huang, J., Kontar, E. P., Nakariakov, V. M., & Gao, G. 2016, ApJ, 831, 119
Inglis, A. R., Ireland, J., & Dominique, M. 2015, ApJ, 798, 108
Inglis, A. R., Nakariakov, V. M., & Melnikov, V. F. 2008, A&A, 487, 1147
Kim, S., Nakariakov, V. M., & Shibasaki, K. 2012, ApJL, 756, L36
Kumar, P., Innes, D. E., & Inhester, B. 2013, ApJL, 779, L7
Kumar, P., Nakariakov, V. M., & Cho, K.-S. 2015, ApJ, 804, 4
Lemen, J. R., Title, A. M., Akin, D. J., et al. 2012, SoPh, 275, 17
Li, D., Yuan, D., Su, Y. N., et al. 2018, A&A, 617, A86
Lin, R. P., Dennis, B. R., Hurford, G. J., et al. 2002, SoPh, 210, 3
Liu, R. 2013, MNRAS, 434, 1309
Liu, W., Chen, Q., & Petrosian, V. 2013, ApJ, 767, 168
Longcope, D., Unverferth, J., Klein, C., McCarthy, M., & Priest, E. 2018, ApJ, 868, 148
Mandal, S., Yuan, D., Fang, X., et al. 2016, ApJ, 828, 72
McLaughlin, J. A., De Moortel, I., Hood, A. W., & Brady, C. S. 2009, A&A, 493, 227
McLaughlin, J. A., Nakariakov, V. M., Dominique, M., Jelínek, P., & Takasao, S. 2018, SSRv, 214, 45
McLaughlin, J. A., Verth, G., Fedun, V., & Erdélyi, R. 2012, ApJ, 749, 30
Nakajima, H., Nishio, M., Enome, S., et al. 1994, IEEEP, 82, 705
Nakariakov, V. M., Foullon, C., Verwichte, E., & Young, N. P. 2006, A&A, 452, 343
Nakariakov, V. M., & Melnikov, V. F. 2009, SSRv, 149, 119
Patsourakos, S., Vourlidas, A., & Stenborg, G. 2013, ApJ, 764, 125

Pesnell, W. D., Thompson, B. J., & Chamberlin, P. C. 2012, SoPh, 275, 3
Pugh, C. E., Broomhall, A. M., & Nakariakov, V. M. 2017, A&A, 602, A47
Pugh, C. E., Broomhall, A.-M., & Nakariakov, V. M. 2019, A&A, 624, A65
Reznikova, V. E., & Shibasaki, K. 2011, A&A, 525, A112
Ruan, W., Xia, C., & Keppens, R. 2019, ApJL, 877, L11
Simões, P. J. A., Hudson, H. S., & Fletcher, L. 2015, SoPh, 290, 3625
Su, Y., Veronig, A. M., Holman, G. D., et al. 2013, NatPh, 9, 489
Sun, J. Q., Cheng, X., & Ding, M. D. 2014, ApJ, 786, 73
Takasao, S., & Shibata, K. 2016, ApJ, 823, 150
Thurgood, J. O., Pontin, D. I., & McLaughlin, J. A. 2017, ApJ, 844, 2
Tian, H., Young, P. R., Reeves, K. K., et al. 2016, ApJL, 823, L16
Torrence, C., & Compo, G. P. 1998, BAMS, 79, 61
Van Doorsselaere, T., Kupriyanova, E. G., & Yuan, D. 2016, SoPh, 291, 3143

Wang, T. 2011, SSRv, 158, 397
Wang, T. J., Solanki, S. K., Curdt, W., et al. 2003a, A&A, 406, 1105
Wang, T. J., Solanki, S. K., Innes, D. E., Curdt, W., & Marsch, E. 2003b, A&A, 402, L17
Warren, H. P., Brooks, D. H., Ugarte-Urra, I., et al. 2018, ApJ, 854, 122
Wu, Z., Chen, Y., Huang, G., et al. 2016, ApJL, 820, L29
Yuan, D., Nakariakov, V. M., Chorley, N., & Foullon, C. 2011, A&A, 533, A116
Yuan, D., Su, J., Jiao, F., & Walsh, R. W. 2016, ApJS, 224, 30
Yuan, D., Van Doorsselaere, T., Banerjee, D., & Antolin, P. 2015, ApJ, 807, 98
Zhao, X., Xia, C., Van Doorsselaere, T., Keppens, R., & Gan, W. 2019, ApJ, 872, 190